Int J Adv Manuf Technol (2016) 85:1969–1982
DOI 10.1007/s00170-016-8635-z

ORIGINAL ARTICLE

Experimental investigation of underwater laser beam micromachining (UW-LBμM) on 304 stainless steel

Rasmi Ranjan Behera[1] · **Mamilla Ravi Sankar**[1] · **J. Swaminathan**[2] · **Indrajeet Kumar**[3] · **Ashwini Kumar Sharma**[3] · **Alika Khare**[3]

Received: 19 August 2015 / Accepted: 17 March 2016 / Published online: 6 April 2016

Abstract Fabrication of miniaturized components provides a challenge to the manufacturing industries and to meet the challenges many unconventional machining methods are developed, among which laser beam micromachining (LBμM) is one. But, thermal effects such as recast layer, heat-affected zone (HAZ), debris, and thermal cracks are commonly observed in LBμM. So, in order to minimize the thermal effects, underwater laser beam micromachining (UW-LBμM) came into existence. In this paper, experiment on UW-LBμM is reported using a Q-switched Nd:YAG laser for fabricating microchannels on 304 stainless steel. The effect of input process parameters (scanning speed, number of scan, laser pulse energy) on output responses (kerf width, kerf depth, surface roughness) of microchannel is studied. Laser micromachined channels are characterized by using optical microscopy, surface profilometer, scanning electron microscopy, and energy dispersive X-ray spectroscopy. It is observed that the dimensions of kerf width and kerf depth are low at lower number of scan, laser pulse energy, and higher scanning speed. The surface roughness decreases with decrease in number of scan and increase in laser pulse energy. Minimum surface roughness is achieved at scanning speed of 300 μm/s. The recast layer and debris are minimum during UW-LBμM compared to LBμM. Elemental comparison is carried out inside and in the surroundings of microchannel.

✉ Mamilla Ravi Sankar
evmrs@iitg.ernet.in

[1] Department of Mechanical Engineering, IIT Guwahati, Guwahati 781039, India

[2] National Metallurgical Laboratory, Jamshedpur 831007, India

[3] Department of Physics, IIT Guwahati, Guwahati 781039, India

Keywords Microchannel · Nd:YAG laser · UW-LBμM · Recast layer · HAZ

1 Introduction

Fabrication of miniaturized products is the subject of intense research, as the applications of these components vary from industry to industry like aerospace, automobile, biomedical, chemical, foundry, and microelectromechanical system (MEMS) [1, 2]. These components include microholes, microchannels, micronozzles, and micromixtures of size less than 500 μm which are commonly found in various microfluidic devices. Because of high thermal conductivity and high strength, metallic microchannels are frequently used for fabricating of microfluidic devices to prevent thermal damages and to support life span of devices [3]. It is very difficult to fabricate the microfeatures in a large number using conventional machining processes due to high tool wear, high heat generation, and mechanical stress in the material. Fabrication of such miniaturized components provides a challenge to the manufacturing industries, and to meet the challenges, many unconventional machining methods are developed, among which laser beam micromachining (LBμM) is one. The main advantages of LBμM are no tool wear, ability to micromachine complex shapes, high precision, and less machining time. As LBμM is a noncontact process, so, it does not exert any mechanical force on the workpiece resulting in a relatively higher process yield and productivity [4].

During LBμM, when a laser beam is focused on the surface of workpiece material, the material in the focal volume is subjected to different physical phenomena such as heating, softening/melting, vaporization, and explosive removal [5, 6]. The physical phenomenon of LBμM is complicated because laser-material interaction depends on laser parameters

(power density, wavelength, pulse duration, laser pulse repetition rate), material properties (thermal conductivity, thermal absorption coefficient), machining parameters (scanning speed, number of scans), and machining medium (gas, liquids) [7–10]. There are a number of drawbacks of LBμM process such as recast layer, heat-affected zone (HAZ), debris, crack formation, and tapering of microcomponent [11–14].

In order to obtain high-quality products, i.e., products with minimum recast layer, HAZ, and debris, post-processing is required, which add cost to the micromachined products [15]. Pulse duration is an important factor which controls the quality of micromachining. Longer pulses generate more bulky and massive removal of workpiece material with less precision as well as high thermal damage. So, shorter pulse duration lasers (nanoseconds to femtoseconds) are used for high precision industrial applications. Femtosecond lasers have produced little contamination and low HAZ due to short beam material interaction time [16]. However, the femtosecond laser micromachining system is costly and machining rates are low compared to nanosecond laser. Thus, nanosecond pulse laser is widely used for micromachining. Furthermore, to reduce the thermal effect such as recast layer, HAZ, debris, and thermal crack, underwater laser beam micromachining (UW-LBμM) came into existence.

Recently, there have been increasing studies on under liquid laser beam micromachining (UL-LBμM) of different materials including metals, alloys, ceramics, glass, semiconductors, composites, and polymer by using different liquids. Commonly used liquid is water, as it is low cost, easily available, and transparent for laser transmission [17–22]. The mechanisms of UW-LBμM for various lasers are different due to change in absorption coefficient of water at different wavelengths. The absorption coefficient of water for 10.6-μm wavelength CO_2 laser, 1.06 μm, and 532-nm wavelength Neodymium-doped Yttrium Aluminum Garnet (Nd:YAG) laser are 500, 0.148, and 0.0005 cm^{-1}, respectively [23–25]. Due to high absorption of water for 10.6-μm wavelength CO_2 laser, a larger portion of laser energy vaporizes the water and forms a conical keyhole along the water thickness to allow laser beam to reach workpiece material surface [23]. Therefore, Nd:YAG laser is used as ideal tool for UL-LBμM because of its low optical energy absorption loss in water. The optical energy absorptivity of most metals is low in near-infrared region but increases with decrease in wavelength. However, there is reduction of maximum laser power available with decrease in wavelength. Thus, visible-wavelength laser like Nd:YAG laser (532 nm) is suitable for the micromachining of metals with nanosecond laser pulses [26].

Kruusing [27, 28] investigated the advantages of water-assisted laser processing and found that underwater laser processing can be applied to cutting, drilling, micromachining, welding, etching, cleaning, and laser shock processes. Both efficiency and quality of LBμM can be greatly improved during underwater laser drilling of copper, iron, aluminum, and stainless steel compared to that of air [29]. The cooling effect of water can reduce the extent of HAZ and microcracks, which are common during micromachining in air. High aspect ratio through hole with reduction of defects like bulges, debris, cracks, scorch, and HAZ was achieved during underwater CO_2 laser drilling of glass [30]. Physical phenomena such as water convection and bubbles generation remove the recast as well as debris from the machining area.

Muhammad and Li [17] reported micromachining of nitinol tube for coronary stent application by using underwater femtosecond laser and found minimum surface roughness at low fluence as well as high speed during micromachining in air. HAZ is obtained at the highest fluence and it reduces with decrease in fluence. But, in UW-LBμM, high surface quality is obtained even at high fluence and low speed. Microchannel without HAZ, debris, recast, and clean back wall is obtained during UW-LBμM.

Narrower kerf width, lower surface roughness, absence of back wall damages, smaller HAZ, and less dross can be obtained in the case of wet fiber laser profile cutting of thin stainless steel tube compared to dry cutting [18]. Due to influence of water dynamics, high recoil pressure is induced, which ejects molten material from the cavity and prevent resolidification layer [23]. Nath et al. [31] fabricated through hole in thin stainless steel sheet by using Nd:YAG laser drilling in air as well as underwater. It was found that laser drilling in water can be done when workpiece is placed above the focal point. UW-LBμM improves heat conduction, increases plasma-induced recoil pressure, weakens the plasma shielding effect in water, and collapses the cavitation bubbles [32]. Krstulovic et al. performed underwater laser ablation of aluminum using pulsed Nd:YAG laser and compared the effect of different

Table 1 Elemental composition of 304 stainless steel

Elements	C	Mn	S	P	Si	Ni	Cr	Fe
Max. %	0.058	1.160	0.005	0.034	0.440	8.080	18.260	Balance

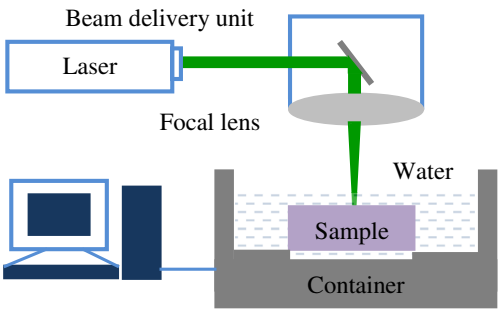

Fig. 1 Schematic diagram of underwater Nd:YAG laser beam micromachining experimental setup

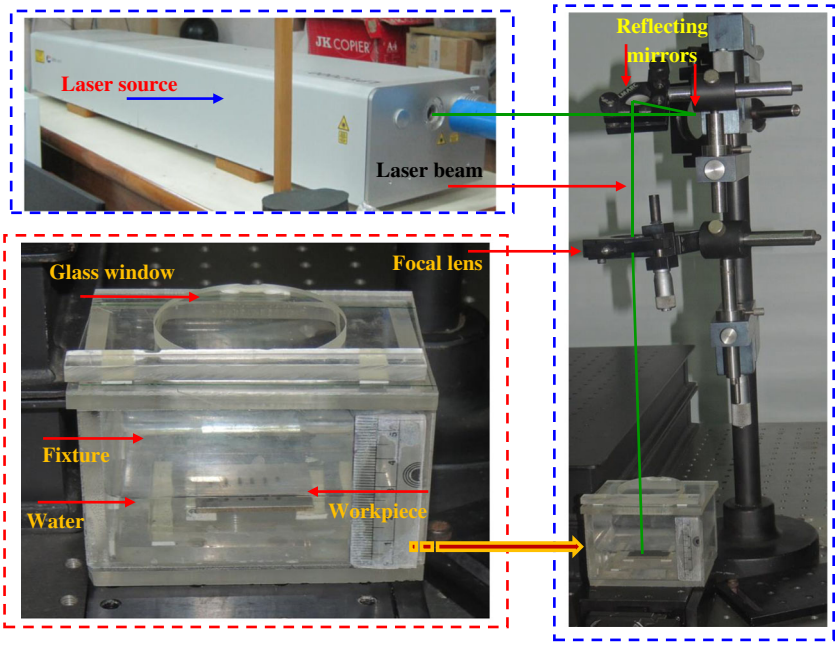

Fig. 2 Photograph of underwater Nd:YAG laser beam micromachining experimental setup

water layer thickness with air. It was observed that underwater laser drilling provides better efficiency as well as better quality holes in terms of shape, volume, and roughness compared to drilling in air [33].

As seen from the above literature review, less work is done regarding performance of Q-switched Nd:YAG UW-LBμM to fabricate microchannel in stainless steel. In the present study, experiments are carried out to investigate UW-LBμM of 304 stainless steel. The effect of water on quality of microchannel is studied and compared with those obtained in air. Besides water effect, the effects of scanning speed, number of scans, and laser pulse energy on microchannel width, depth, and surface roughness are investigated.

2 Experimental methodologies

2.1 Materials

The 304 stainless steel (SS 304) sheet metal (50 × 20 × 2 mm) is used as the specimen in the present research work. The elemental composition for the material is given in Table 1.

2.2 Experimental setup

The schematic diagram of UW-LBμM system is shown in Fig. 1. The Q-switched Nd:YAG pulsed laser with wavelength of 532 nm is used for micromachining. This laser micromachining system consists of various subsystems like laser source, beam delivery unit, power supply unit, Q-switch driver unit, and cooling unit. The output from Q-switched Nd:YAG laser is delivered to workpiece through a series of reflecting mirrors and a convergent lens with a focal length of 250 mm to a laser spot size of 100 μm approximately on the surface of specimen. The pulse duration and pulse frequency of laser beam are 10 ns and 10 Hz, respectively. The laser pulse energy is measured by energy meter, before the laser beam passes through focusing lens.

2.3 Experimental procedure

Fabrication of microchannels is carried out on SS 304 using water as liquid medium. Before micromachining, the sample surface is polished and cleaned with acetone in order to remove any oil and dust. The workpiece is fixed with the container and immersed horizontally in a water bath with thickness of 10 mm, i.e., the thickness of water above the workpiece surface is 10 mm. The water depth is controlled at a particular thickness above the workpiece surface by the total volume method whose depth is proportional to the volume at a constant area of the container. In order to obtain 10-mm thickness of water above the workpiece surface, 120 ml of water is maintained in the container. The container is designed

Table 2 Experimental input parameters and their ranges

Input parameters	Unit	Ranges
Scanning speed (SS)	μm/s	150–400
Number of scans (NOS)	–	10–60
Laser pulse energy (LPE)	mJ	30–80
Water layer thickness (WH)	mm	10

according to the space available in setup and is made up of acrylic polymer. During the experiment, some splashing of water occurs which is very negligible. In order to prevent the splashing of water onto focusing lens, the fixture is covered by glass window (Fig. 2). Thus, whatever amount of water splashes, that amount of water remains in the container. During experiment, some amount of water is absorbed, but this amount is too negligible, because water absorption coefficient for 532 nm wavelength Nd:YAG laser is very less ($0.0005\ cm^{-1}$). So, the thickness of water is almost constant during experiments. The container is placed on a motorized XY translation stage to enable laser scanning. During experiments, microchannels are machined on SS 304 by focusing the laser beam on workpiece surface and moving it with respect to workpiece in a reciprocating motion for a distance of 5 mm.

In the presence of water, the focal length of lens increases with water height level. The increase is approximately 0.33 h,

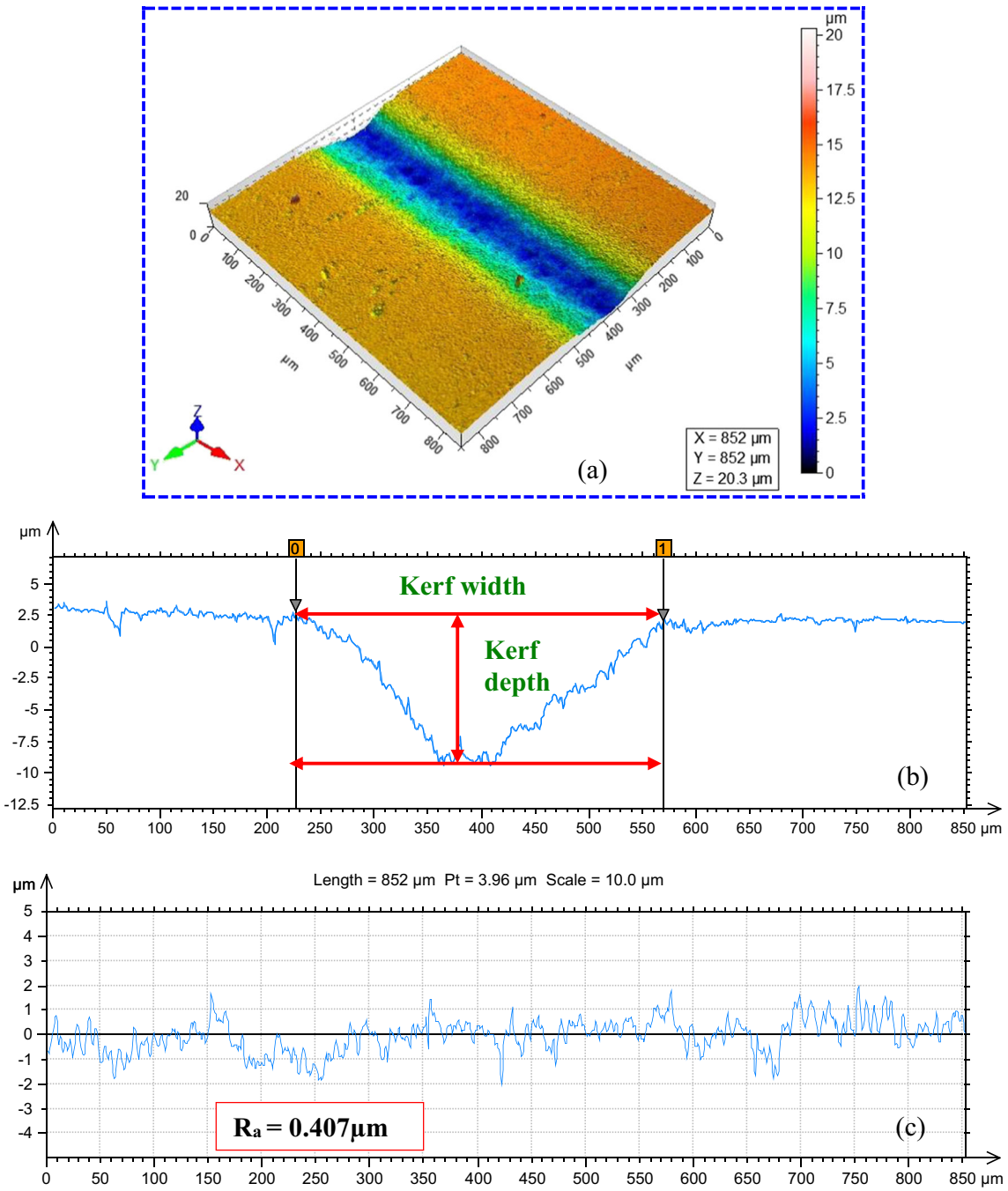

Fig. 3 Surface topography of microchannel using UW-LBµM: **a** 3D surface of microchannel, **b** kerf width and depth, and **c** surface roughness plot of the microchannel along the longitudinal direction (LPE = 80 mJ, SS = 300 µm/s, WH = 10 mm, NOS = 30)

where h is the height of water level above the focal point in air [31, 32]. UW-LBμM is carried out by changing the position of workpiece with respect to focal point of the lens. Scanning speed (SS), number of scans (NOS), and laser pulse energy (LPE) are varied in the experiments, and their ranges are shown in Table 2. To study the influence of one parameter on output responses, the particular parameter is varied by keeping other two parameters at one of the middle value of their ranges. Same is followed for all other input parameters. All the experiments are carried out at room temperature. The laser micromachining in air is also performed as a reference sample for comparison. The output responses such as kerf width, kerf depth, and surface roughness are observed. The kerf width, depth, and surface roughness of microchannels are measured by using 3D surface profilometer. For reducing the errors during measurement, every response is measured at five different locations across the channel, and their statistical average is recorded as the output.

It is found that as the scanning speed is set at a higher range, there is no continuous channel as the percentage of overlapping is less. At lower scanning speed, the kerf width and surface roughness are much more. Hence, scanning speeds are set in a range of 150–400 μm/s. It is observed that at lower number of scans, the microchannel is not formed and, at higher number of scans, average surface roughness obtained is high. So, the number of scans is considered in between 10 and 60. In order to achieve the desired microchannel with set scanning speed and number of scans, the laser pulse energy is selected in the range of 30–80 mJ. The laser fluences can be determined by using the values of pulse energy and laser beam diameter at workpiece surface. The laser spot size on the surface of specimen in air is 100 μm approximately. Thus, the laser fluences obtained are 382, 509, 637, 764, 891, and 1019 J/cm^2 for different laser pulse energies of 30, 40, 50, 60, 70, and 80 mJ, respectively. The microchannels are subsequently characterized by using scanning electron microscopy (SEM) and optical microscopy. SEM and optical microscopy are employed to analyze the morphology as well as microstructure of laser micromachined region. Energy dispersive X-ray spectroscopy (EDS) is performed for elemental analysis at different micromachined zones in the material during UW-LBμM.

3 Results and discussion

The surface topography of microchannel that micromachined on SS 304 using UW-LBμM is shown in Fig. 3. The 3D view of microchannel that shows all the details is represented in Fig. 3a. The kerf width (horizontal distance of the microchannel) and kerf depth (vertical distance between bottom surface of microchannel and normal workpiece surface) details are shown in Fig. 3b. The roughness plot of microchannel measured along the longitudinal direction of microchannel is shown in Fig. 3c.

3.1 Effect of water medium on laser micromachining of 304 stainless steel

Figure 4 shows the 3D surface profilometry images of microchannel in SS 304 during LBμM in air and in water. It can be observed that the recast layer height present along the microchannel is nearly 0.3 mm during LBμM in air (Fig. 4a); however, it is very less or absent on surface of microchannel during UW-LBμM (Fig. 4b).

When high energy laser pulses are focused on material surface, it melts, vaporizes, and ionizes the material in focal volume, resulting in the formation of plasma. When this plasma expands, a recoil pressure is exerted on workpiece surface, causing material removal. During LBμM, the rapid heating as well as cooling cycles lead to formation and resolidification of molten steel within each pulse duration. Thus, recast layer and debris are formed which cannot be ejected away from the micromachined region and deposited on bottom as well

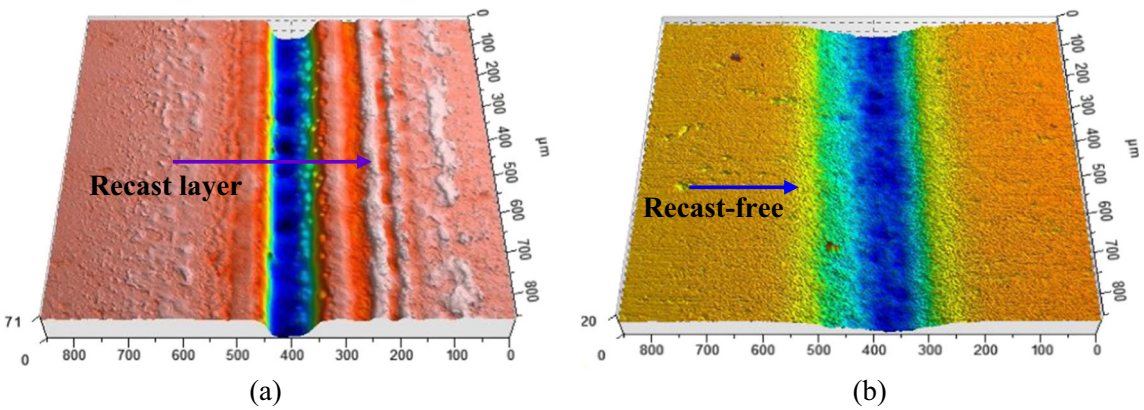

Fig. 4 Surface profilometry images of microchannel during LBμM **a** in air and **b** in water (LPE = 80 mJ, NOS = 30, SS = 300 μm/s)

as periphery of the microchannel. Figure 5 shows SEM images of microchannel during LBμM and UW-LBμM of stainless steel. In the case of laser micromachining in air, resolidified layer and debris are found accumulating at the bottom and surrounding of microchannel (Fig. 5a). Cracks are also found on the surrounding of microchannel in resolidified region. But, in the case of UW-LBμM, a better quality microchannel is formed with debris-free and recast-free (Fig. 5b). These debris and recast layer degrade the quality as well as

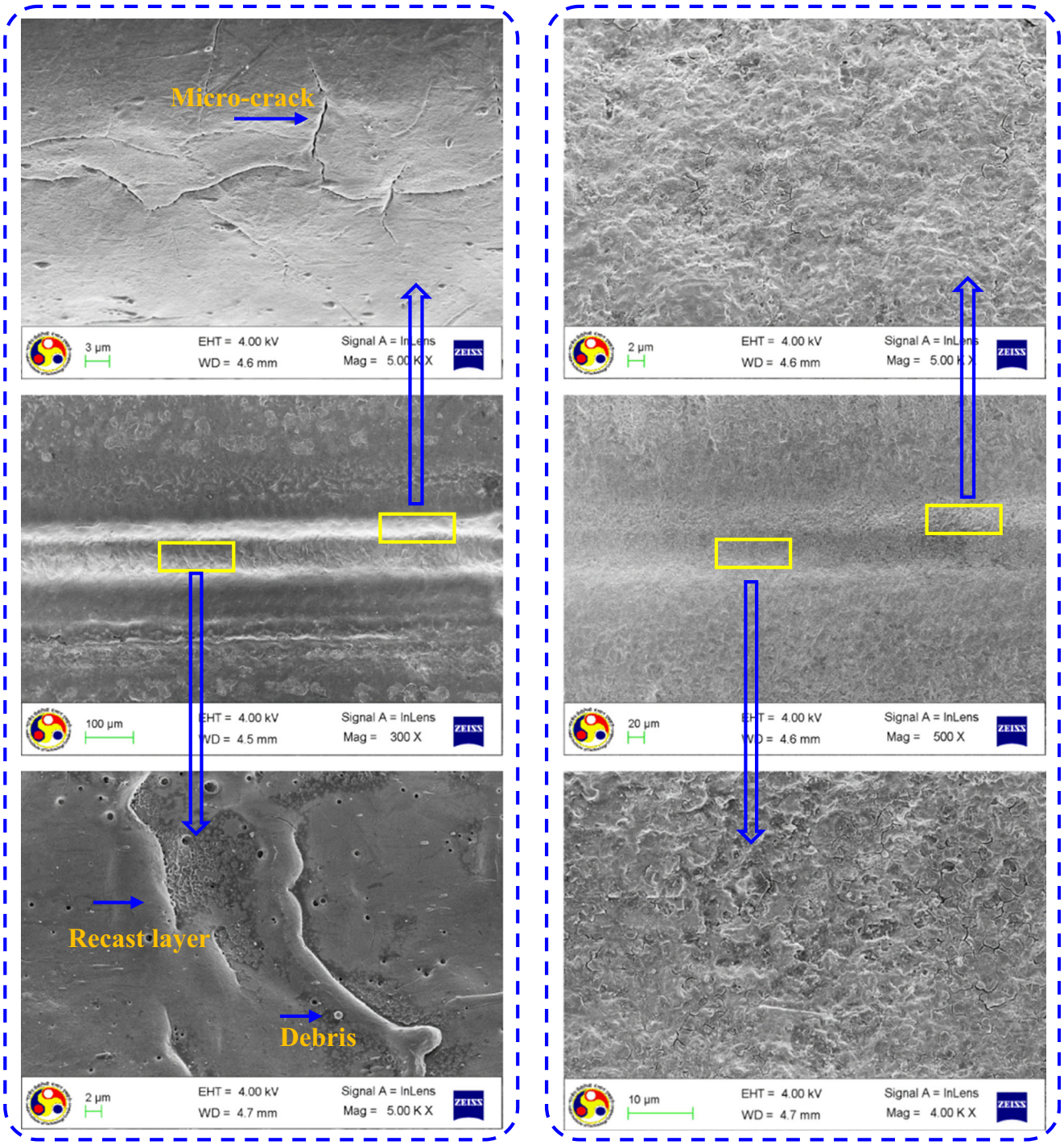

Fig. 5 Surface morphology of microchannels: **a** presence of recast layer, debris, and microcracks on the surrounding and bottom part of microchannel during LBμM in air **b** recast-free and debris-free microchannel during UW-LBμM

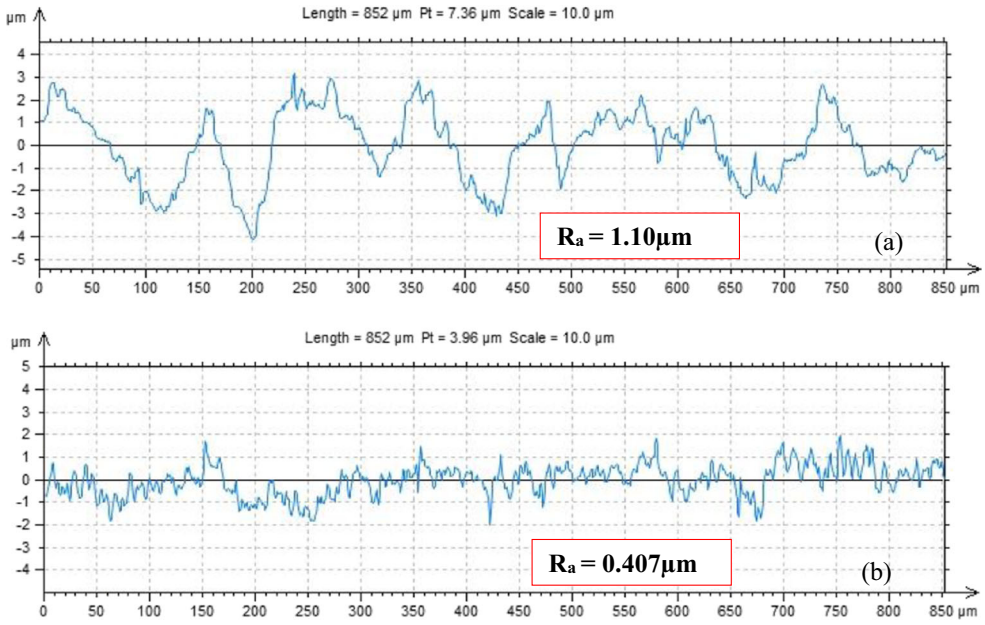

Fig. 6 Roughness plot of bottom surface of the microchannel **a** in air and **b** in water (LPE = 80 mJ, SS = 300 µm/s, NOS = 30)

functionality of the components. Due to rapid heating and cooling, thermal stress is occurred which results in the formation of cracks.

During UW-LBµM, when high energy laser pulses are focused on the material surface through water medium, high temperature and high pressure plasma is generated as well as expanded. This expansion of plasma is confined by underwater pressure and leads to an increase in plasma-induced pressure. This increase of plasma-induced pressure ejects the molten phase of material from ablated region, making the microchannel free of redeposited material. In addition, the plasma transfers its energy to water. This energy transfer is strong enough to induce phase transition in water, i.e., vaporization of water. So, a large number of bubbles are generated in the water. The molten particles are carried out by convection of bubble motion. Furthermore, due to collapsing of bubbles near the sample surface, a high speed liquid jet is generated to produce a strong impulse toward sample surface, which helps in expulsion of molten material. Thus, due to strong plasma expansion, vaporization of water, and collapsing of bubbles, the recast layer and debris are ejected away from micromachining region during UW-LBµM.

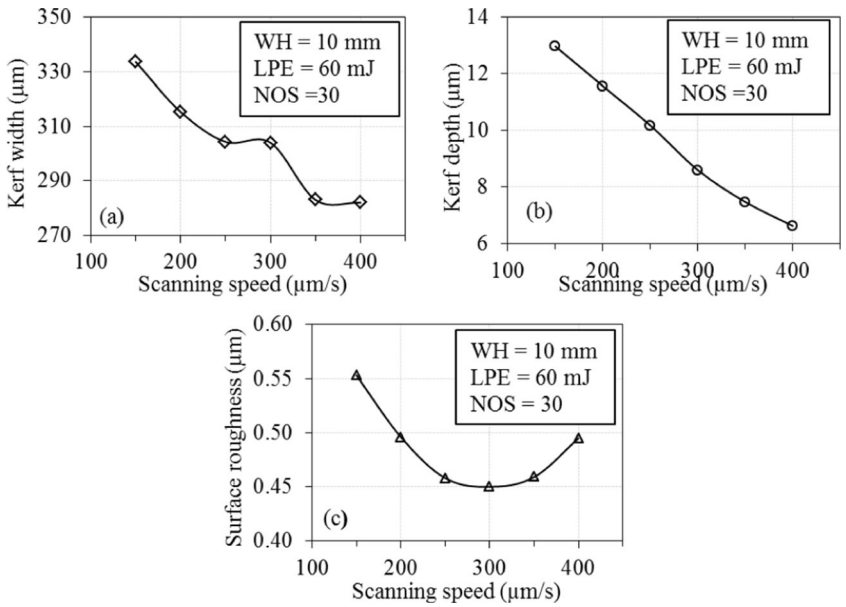

Fig. 7 Effect of scanning speed on microchannel quality characteristics: **a** kerf width, **b** kerf depth, and **c** surface roughness, R_a (WH = 10 mm, NOS = 30, LPE = 60 mJ)

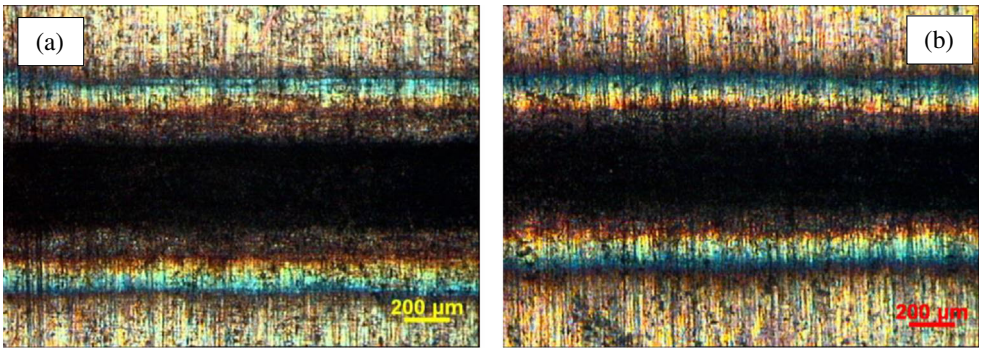

Fig. 8 Optical microscopy photographs of microchannels at different scanning speeds: **a** SS = 150 µm/s and **b** SS = 400 µm/s

The roughness of bottom surface of microchannel machined in air and water is shown in Fig. 6a, b. The average surface roughness (R_a) of bottom surface micromachined in air (R_a = 1.10 µm) is approximately 2.7 times higher than that of the bottom surface micromachined in water (R_a = 0.407 µm). This is due to the presence of recast layer, debris, and adherence of dross on the bottom surface during LBµM in air (Fig. 6a). The convective flow and bubble-induced motion of water ejects molten material as well as debris from the irradiated zone. This prevents resolidification on surrounding and bottom part of the microchannel. Thus, relatively smooth surface is obtained during UW-LBµM (Fig. 6b).

3.2 Effect of scanning speed on microchannel quality characteristics

The effect of scanning speed on microchannel kerf width, kerf depth, and R_a is shown in Fig. 7 (water height (WH) = 10 mm, NOS = 30, LPE = 60 mJ). It can be seen that both the kerf dimensions, i.e., kerf width and kerf depth, decrease with increase in scanning speed (Fig. 7a, b). This is mainly due to increase in scanning speed, and the interaction time between laser and workpiece material reduces, which decreases heat transfer to material in both directions (i.e., radially outward as well as vertically downward directions). This leads to decrease in melting and vaporization which reduces kerf width as well as kerf depth. Because of reduction in melting and evaporation, kerf width reduces from 334 to 282 µm and kerf depth from 13 to 6 µm as scanning speed increases from 150 to 400 µm/s.

Figure 7c shows the influences of the scanning speed on R_a. The R_a decreases from 0.553 to 0.450 µm as scanning speed increases from 150 to 300 µm/s. Recast layer plays an important role in microchannel surface roughness. When laser beam interacts with the material, melting occurs which forms molten pool. This molten pool cools and solidifies before the material surface cools. So, it retains its surface texture on the material. Due to bubble-induced motion and convective motion of liquid during UW-LBµM, the recast layer and debris are ejected out from bottom part of microchannel. When scanning speed increases, less melting occurs with formation of less recast layer as well as debris due to less interaction between

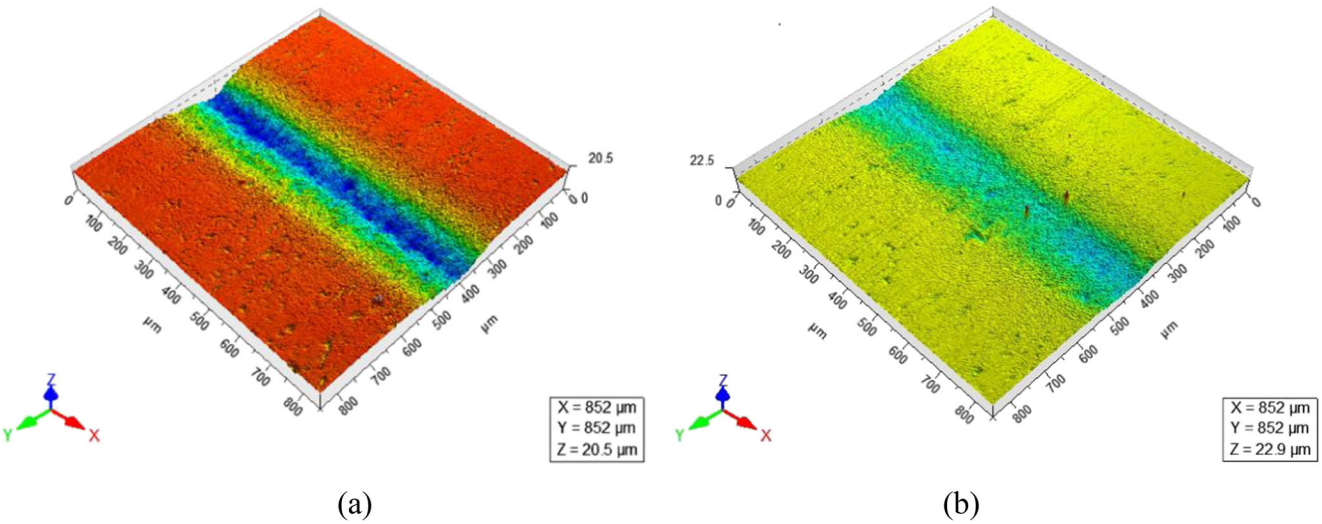

Fig. 9 Three-dimensional surface profiles of microchannels at different scanning speeds: **a** SS = 150 µm/s and **b** SS = 400 µm/s

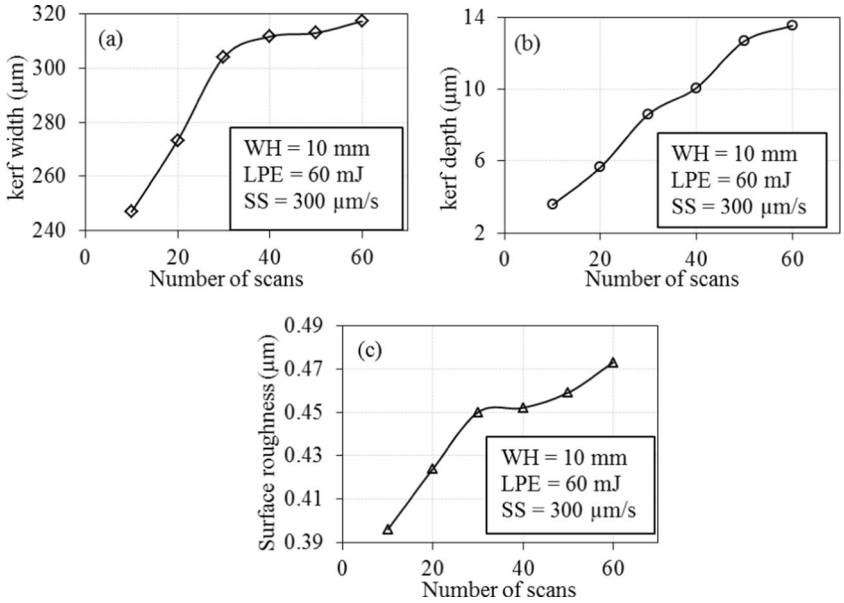

Fig. 10 Effect of number of scans on microchannel quality characteristics: **a** kerf width, **b** kerf depth, and **c** surface roughness, R_a (WH = 10 mm, SS = 300 μm/s, and LPE = 60 mJ)

laser and material. Furthermore, due to less melting, the irregularity of molten pool also decreases. Thus, due to decrease in irregularities of molten pool, the roughness also decreases with increase in scanning speed. After 300 μm/s, the surface roughness gradually increases because nonuniform melting is more pronounced at higher scanning speed due to lack of overlapping of pulses as well as very low interaction between laser and workpiece material. So, surface is more rough at higher scanning speed.

Figures 8 and 9 show the corresponding optical microscope and surface profilometer photographs of microchannels at different scanning speeds ((a) SS = 150 μm/s and (b) SS = 400 μm/s). It is clearly seen that for higher scanning speed, the kerf width and depth are smaller. This is mainly because of less heat transfer at higher scanning speed due to less interaction time between laser and workpiece material. The debris are absent at the surrounding of the microchannel due to bubble-induced motion and convective motion of liquid during UW-LBμM.

3.3 Effect of number of scans on microchannel quality characteristics

Figure 10 shows the microchannel quality characteristics as a function of number of scans at constant WH = 10 mm, SS = 300 μm/s, and LPE = 60 mJ. It is clearly observed that the kerf width increases from 247 to 304 μm as the number of scans increases from 10 to 30 (Fig. 10a). However, variation of kerf width is negligible (304 to 317 μm) when there is increase in number of scans from 30 to 80. This is because the effective laser micromachined surface on workpiece mainly depends on laser pulse energy and scanning speed. When laser pulse energy increases, the heat transfer to material increases, so, more surface area is affected; this leads to larger kerf width. Similarly, when scanning speed increases, the interaction time between laser beam and workpiece material decreases, thus less surface area is subjected to melting, and hence smaller kerf width is observed. But, when all these parameters keep unchanged and only the number of scans increases, the effective surface area subjected to melting rapidly reaches to its peak value. So, kerf width increases. After

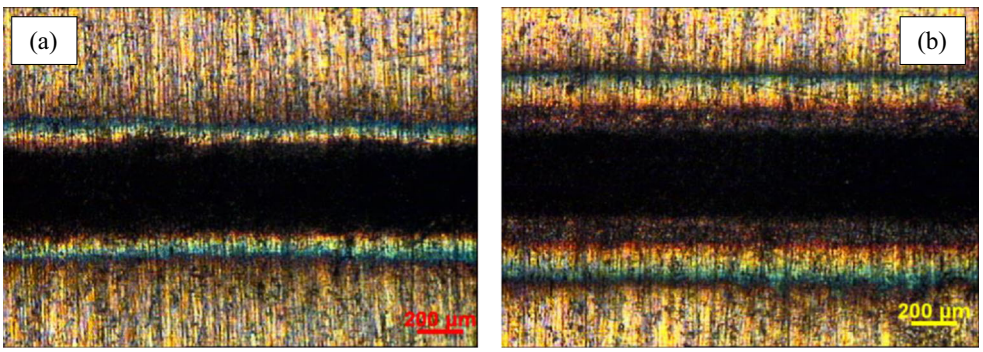

Fig. 11 Optical microscopy photographs of microchannels at different scanning pass numbers: **a** NOS = 10 and **b** NOS = 60

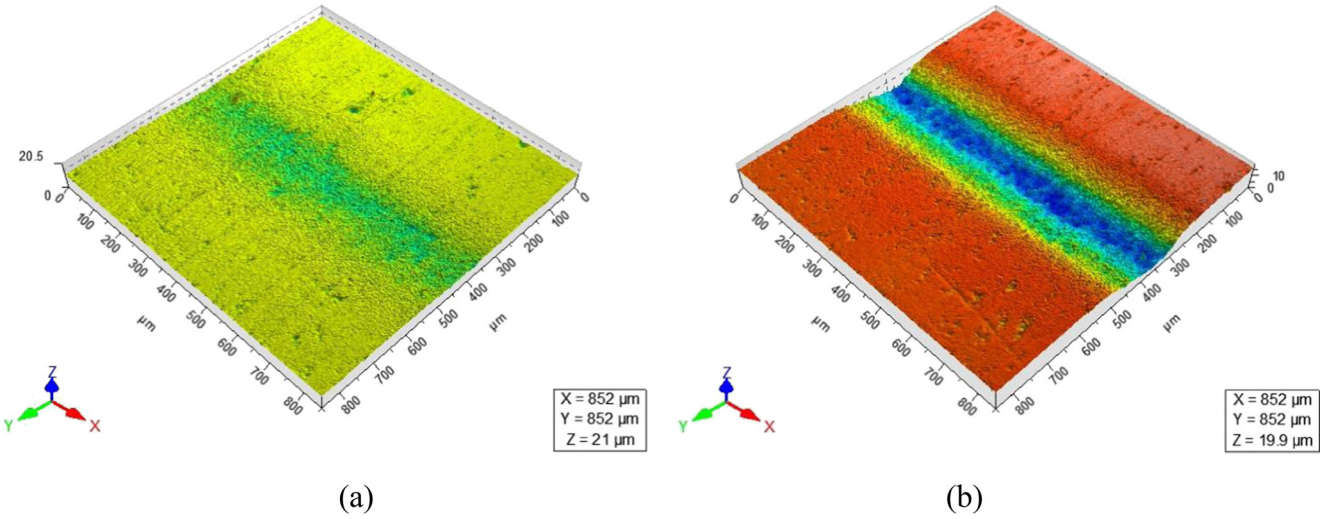

Fig. 12 Three-dimensional surface profiles of microchannels at different number of scans: **a** NOS = 10 and **b** NOS = 60

that, the effective area on the workpiece surface makes no significant change with increase in number of scans because the heat transfer occurs only in thickness direction. Thus, kerf width remains approximately constant, and only kerf depth increases.

Figure 10b shows the relationship between kerf depth and number of scans. It is observed that the kerf depth is directly proportional to number of scans. As scanning number increases from 10 to 60, the kerf depth increases from 3 to 14 μm due to gradual melting and evaporation of material for each scanning pass.

Figure 10c shows the effect of number of scans on surface roughness. The surface roughness increases from 0.396 to 0.473 μm as number of scans varies from 10 to 60. Due to more melting and vaporization of material that occur by gradually increasing the number of scans, the irregularities in molten pool increase for each scan. Thus, the surface becomes rougher gradually as number of scans increases.

Figures 11 and 12 show the optical microscopy as well as surface profilometry images of microchannels at different number of scan ((a) NOS = 10, (b) NOS = 60). Larger kerf width and depth are observed at higher number of scans.

3.4 Effect of laser pulse energy on microchannel quality characteristics

The effect of laser pulse energy on microchannel quality characteristics is shown in Fig. 13 (WH = 10 mm, SS = 300 μm/s, and NOS = 30). According to Fig. 13a, b, both kerf width and kerf depth are found to be approximately proportional to laser

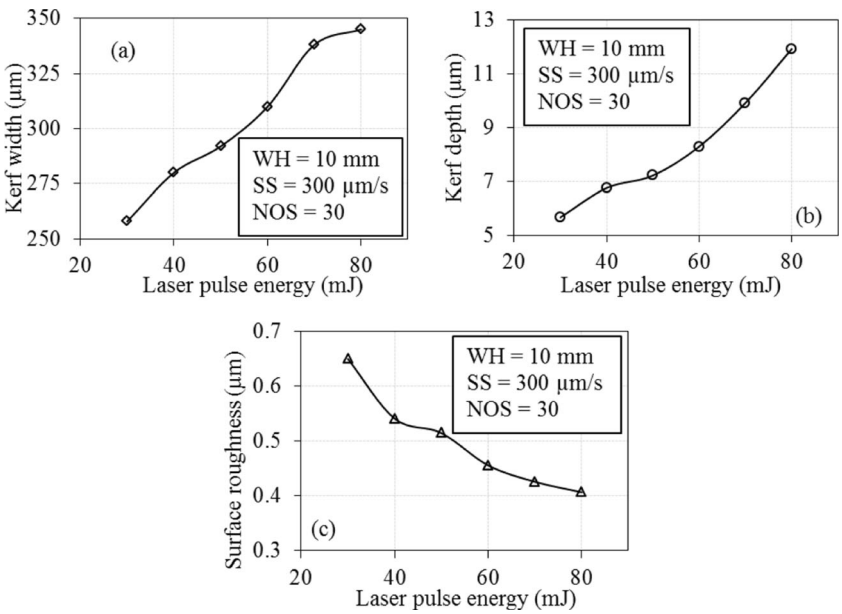

Fig. 13 Effect of laser pulse energy on microchannel quality characteristics: **a** kerf width, **b** kerf depth, and **c** surface roughness, R_a (WH = 10 mm, SS = 300 μm/s, and NOS = 30)

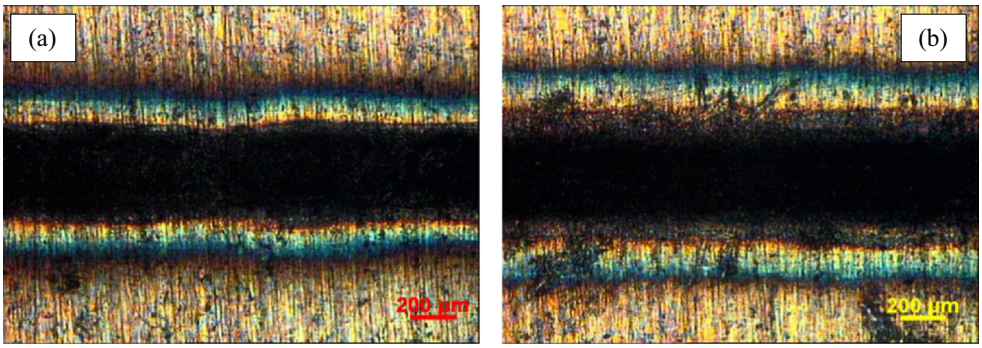

Fig. 14 Optical microscopy photographs of microchannels at different laser pulse energies: **a** LPE = 30 mJ and **b** LPE = 80 mJ

pulse energy. During micromachining process, the average power supplied is controlled by laser pulse energy. The small variation in average power results in a large variation of kerf dimension. The kerf width increases from 250 to 350 µm and kerf depth from 5 to 12 µm as the laser pulse energy increases from 30 to 80 mJ. This phenomenon can be explained that as laser pulse energy increases, the energy density (i.e., energy per unit area) increases. So, heat energy delivered to the material increases. Thus, more melting and vaporization occur, which lead to increase in kerf dimension.

Figure 13c shows the surface roughness as a function of laser pulse energy. The surface quality increases with increase in laser pulse energy. Because of hydrodynamics of water over workpiece surface, the redeposition is prevented as the recast layer and debris are removed away from the cut region by thermally disturbed water layer.

Figures 14 and 15 show the optical as well as surface profilometry images of microchannels at different laser pulse energies, (a) LPE = 30 mJ and (b) LPE = 80 mJ. At 80-mJ laser pulse energy, the kerf width and depth are larger due to high heat transfer to the material as compared to 30-mJ laser pulse energy.

3.5 Metallurgical elemental characterization

Figure 16 shows the energy dispersive spectroscopy (EDS) analysis of different regions of microchannel that are laser beam micromachined in (a) air and (b) underwater. For both the conditions, it can be observed that oxygen level is gradually decreasing with increase in distance from the center of microchannel. Due to "Gaussian" distribution of laser beam, the intensity of laser beam is higher at center portion and gradually decreases toward the edges of microchannel. So, more intensity of heat leads to more oxidization at the central part of laser micromachining zone (i.e., middle of the microchannel). However, the oxygen percentages at different laser beam micromachining regions are less in UW-LBµM as compared to LBµM in air. Because of flow of water, the recast layer and debris which are highly oxidized are ejected away from the ablated regions of microchannel. Also, due to cooling effect of water (high convective heat transfer coefficient compared to air), the intensity of heat is less which leads to less oxidization in UW-LBµM.

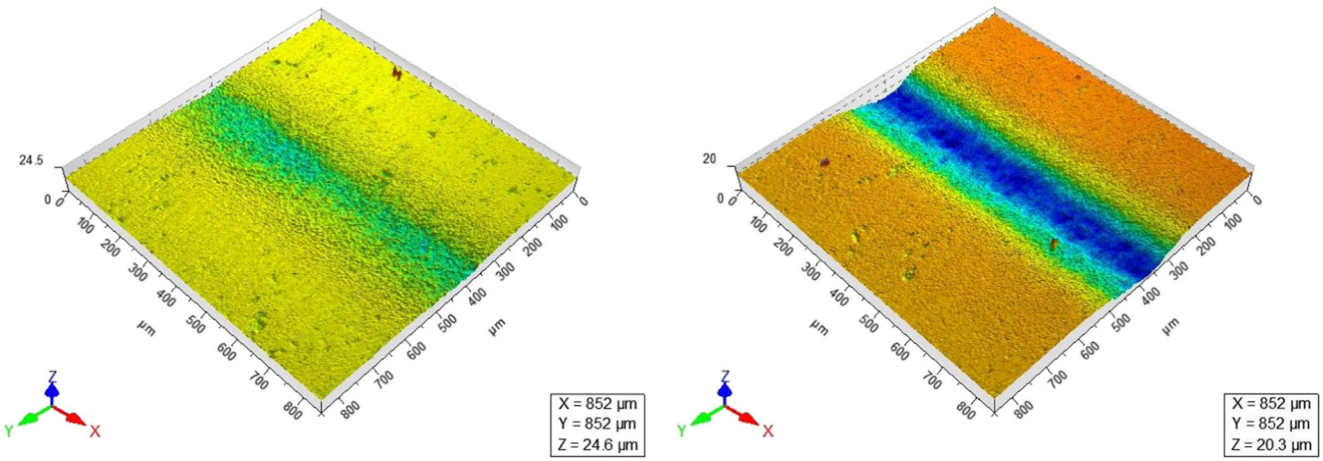

(a) (b)

Fig. 15 Three-dimensional surface profiles of microchannels at different laser pulse energies: **a** LPE = 30 mJ and **b** LPE = 80 mJ

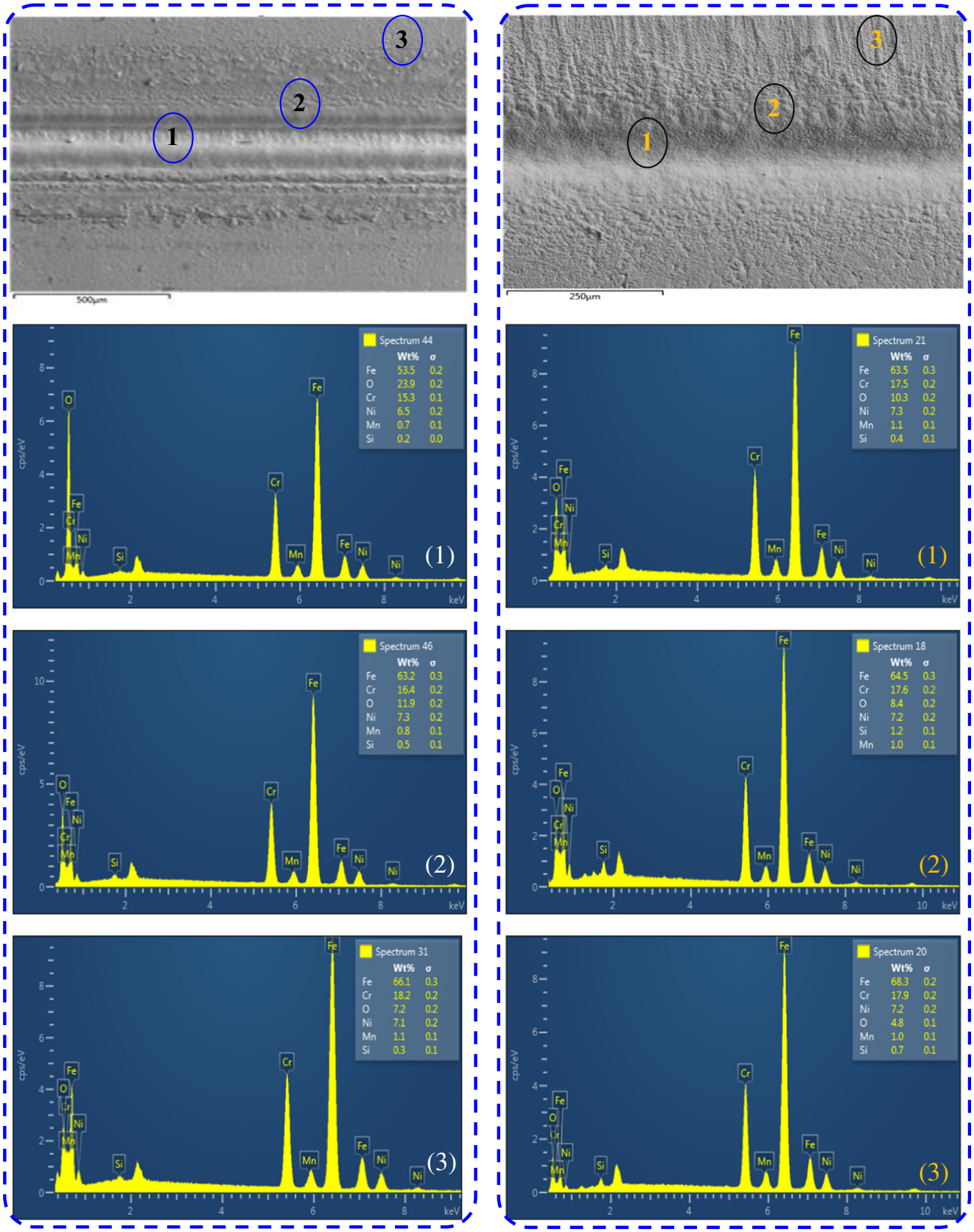

Fig. 16 Laser beam micromachined channel in **a** air, **b** underwater, and corresponding energy dispersive spectroscopy of various regions of microchannel surface

4 Conclusions

UW-LBμM tests are successfully carried out on 304 stainless steel substrate, using Q-switched Nd:YAG laser. It is found that UW-LBμM is the effective method in order to obtain high-quality microchannel with recast-free and debris-free as compared to LBμM in air. Water acts as a cooling medium which results in minimum cracks due to reduction of thermal load. Furthermore, better surface finish as well as cleaner microchannel is obtained during UW-LBμM. Because of strong plasma expansion, vaporization of water, and collapsing of bubbles, the recast layer and debris are ejected away from micromachining region during UW-LBμM. The microchannel quality, roughness, depth, and width are dependent on the ranges of input parameters. With increase in number of scans from 10 to 60 and laser pulse energy from 30 to 80 mJ, kerf width increases from 247 to 345 μm but decreases from 333 to 282 μm when scanning speed varies from 150 to 400 μm/s. Kerf depth is also increased from 3 to 14 μm with increase in number of scans as well as laser pulse energy and decreases from 13 to 6 μm with increase in scanning speed. The surface roughness decreases from 0.65 to 0.40 μm with increase in laser pulse energy but increases from 0.39 to 0.47 μm with increase in laser scan number. With increase in scanning speed up to 300 μm/s, the surface quality improves and then after degrades. The minimum kerf width is obtained at 400 μm/s scanning speed, 10 numbers of scans, and 30-mJ laser pulse energy. The optimized surface quality is obtained at 300 μm/s scanning speed, 10 numbers of scans, and 80-mJ laser pulse energy. The EDS analysis shows that the quantities of oxygen element at different laser beam micromachining regions are less in UW-LBμM as compared to LBμM in air.

Acknowledgments The authors are thankful for the financial support provided by Indian Institute of Technology Guwahati (Project Number: SG/ME/P/MRS/01), Board of Research in Nuclear Sciences (Project Number: ME/P/MRS/02), Department of Electronics & Information Technology (Centre for Excellence in Research and Development of Nanoelectronic Theranostic Devices), Department of Science and Technology for their "Technology Systems Development Programme (DST/TSG/AMT/2015/619)" and Fist project (SR/FST/ETI-244/2008). This paper is a revised and expanded version of the paper entitled "Experimental Study on Micromachining of 304 Stainless Steel Under Water Using Pulsed Nd:YAG Laser Beam" presented at the 5th International & 26th AIMTDR Conference held at IIT Guwahati, Assam, India, last December 12–14, 2014.

References

1. Dahotre NB, Harimkar SP (2008) Laser micromachining. Laser fabrication and machining of materials. Springer, pp 247–288
2. Ghoshal B, Bhattacharyya B (2015) Generation of microfeatures on stainless steel by electrochemical micromachining. Int J Adv Manuf Technol 76:39–50
3. Im H, Oh KH, Kim SG, Jeong S (2009) Application of etchant jet for laser micromachining of metal channels. Int J Precis Eng Manuf 10(4):101–105
4. Kannatey E (2009) Principles of laser materials processing. Wiley, Hoboken
5. Khalil AAI, Sreenivasan N (2005) Study of experimental and numerical simulation of laser ablation in stainless steel. Laser Physics Letter 2(9):445–451
6. Raval A, Choubey A, Engineer C, Kothwala D (2004) Development and assessment of 316LVM cardiovascular stents. Mater Sci Eng A 386:331–343
7. Leone C, Genna S, Caprino G, De Iorio I (2010) AISI 304 stainless steel marking by a Q-switched diode pumped Nd:YAG laser. J Mater Process Technol 210:1297–1303
8. Ahn D, Seo C, Park T, Park D, Park S, Kwon Y, Kim D (2014) Micromachining of stainless steel–polymer composites using nanosecond and femtosecond UV lasers. Int J Adv Manuf Technol 74: 1691–1699
9. Akhtar SN, Choudhary H, Ramakrishna SA, Ramkumar J (2014) Simulations and experiments on excimer laser micromachining of metal and polymer. Journal of Micro/Nanolithography, MEMS, and MOEMS 13(1):013008(1–9)
10. Chen K, Yao YL (2000) Process optimization in pulsed laser micromachining with applications in medical device manufacturing. Int J Adv Manuf Technol 16:243–249
11. Voisey K et al (2003) Melt ejection during laser drilling of metals. Mater Sci Eng A 356(1):414–424
12. Zoppel S, Farsari M, Merz R, Zehetner J, Stangl G, Reider GA, Fotakis C (2006) Laser micro machining of 3C–SiC single crystals. Microelectron Eng 83:1400–1402
13. Ghoreishi M, Low D, Li L (2002) Comparative statistical analysis of hole taper and circularity in laser percussion drilling. Int J Mach Tool Manufact 42(9):985–995
14. Sezer HK, Li L, Schmidt M, Pinkerton AJ, Anderson B, Williams P (2006) Effect of beam angle on HAZ, recast and oxide layer characteristics in laser drilling of TBC nickel superalloys. Int J Mach Tool Manufact 46(15):1972–1982
15. Miller P, Aggarwal R, Doraiswamy A, Lin YJ, Lee YS, Narayan RJ (2009) Laser micromachining for biomedical applications. J Miner Met Mater Soc 61:35–40
16. Pecholt B, Vendan M, Dong Y, Molian P (2007) Ultra laser micromachining of 3C–SiC thin films for MEMS device fabrication. Int J Mach Tool Manufact 39:239–250
17. Muhammad N, Li L (2012) Underwater femtosecond laser micromachining of thin nitinol tubes for medical coronary stent manufacture. App Phys A 107:849–861
18. Muhammad N, Whitehead D, Boor A, Li L (2010) Comparison of dry and wet fibre laser profile cutting of thin 316L stainless steel tubes for medical device applications. J Mater Process Technol 210: 2261–2267
19. Wee LM, Khoong LE, Tan CW, Lim GC (2011) Solvent-assisted laser drilling of silicon carbide. Int J Appl Ceram Technol 8(6): 1263–1276
20. An R, Li Y, Dou Y, Liu D, Yang H, Gong (2006) Water-assisted drilling of microfluidic chambers inside silica glass with femtosecond laser pulses. App Phys A 83:27–29
21. Karimzadeh R, Anvari JZ, Mansour N (2009) Nanosecond pulsed laser ablation of silicon in liquids. App Phys A 94: 949–955
22. Prakash S, Acherjee B, Kuar AS, Mitra S (2013) An experimental investigation on Nd:YAG laser microchanneling on polymethyl methacrylate submerged in water. Proc IMechE B J Eng Manuf 227(4):508–519
23. Yan Y, Li L, Sezer K, Wang W, Whitehead D, Ji L, Bao Y, Jiang Y (2011) CO_2 laser underwater machining of deep cavities in alumina. J Eur Ceram Soc 31:2793–2807

24. Mullick S, Madhukar YK, Kumar S, Shukla DK, Nath AK (2011) Temperature and intensity dependence of Yb-fiber laser light absorption in water. Appl Opt 50:6319–6326
25. Porter JA, Louhisalmi YA, Karjalainen JA, Füger S (2007) Cutting thin sheet metal with a water jet guided laser using various cutting distances, feed speeds and angles of incidence. Int J Adv Manuf Technol 33:961–967
26. Knowles MRH, Rutterford G, Karnakis D, Ferguson A (2007) Micro-machining of metals, ceramics and polymers using nanosecond lasers. Int J Adv Manuf Technol 33:95–102
27. Kruusing A (2004) Underwater and water-assisted laser processing: part 1—general features, steam cleaning and shock processing. Opt Laser Eng 41:307–327
28. Kruusing A (2004) Underwater and water-assisted laser processing: part 2—Etching, cutting and rarely used methods. Opt Laser Eng 41:329–352
29. Lu J, Xu RQ, Chen X, Shen ZH, Ni XW, Zhang SY, Gao CM (2004) Mechanisms of laser drilling of metal plates underwater. J Appl Phys 95(8):3890–3894
30. Chung CK, Lin SL (2010) CO_2 laser micromachined crack less through holes of Pyrex 7740 glass. Int J Mach Tool Manufact 50: 50961–50968
31. Nath AK, Hansdah D, Roy S, Choudhury AR (2010) A study on laser drilling of thin steel sheet in air and underwater. J Appl Phys 107(12):123103(1–9)
32. Mak GY, Lam EY, Choi HW (2011) Liquid-immersion laser micromachining of GaN grown on sapphire. App Phys A 102: 441–447
33. Krstulovic N, Shannon S, Stefanuik R, Fanara C (2013) Underwater-laser drilling of aluminum. Int J Adv Manuf Technol 69:1765–1773